

Article

Not peer-reviewed version

Evidence for Novel Reticular Corpuscle-Connected Filiform Structures Entangled on the Fascia of the Internal Organs of Rats: The Implication for Cell Death

[Byung-Cheon Lee](#)^{*}, Jeong Yim Lee, [Ki-Seok Lee](#), [Inhyung Lee](#), Hoon Gi Kim, [Ki-Bog Lee](#)^{*}

Posted Date: 10 April 2023

doi: 10.20944/preprints202304.0132.v1

Keywords: Fascia; Cell death; Repeatability; Immunohistochemistry; Bonghan duct and corpuscle; Janus Green B



Preprints.org is a free multidiscipline platform providing preprint service that is dedicated to making early versions of research outputs permanently available and citable. Preprints posted at Preprints.org appear in Web of Science, Crossref, Google Scholar, Scilit, Europe PMC.

Copyright: This is an open access article distributed under the Creative Commons Attribution License which permits unrestricted use, distribution, and reproduction in any medium, provided the original work is properly cited.

Article

Evidence for Novel Reticular Corpuscle-Connected Filiform Structures Entangled on the Fascia of the Internal Organs of Rats: The Implication for Cell Death

Byung-Cheon Lee ^{1,*}, Jeong Yim Lee ¹, Ki-Seok Lee ^{2,3}, Inhyung Lee ⁴, Hoon Gi Kim ⁵
and Ki-Bog Lee ^{6,*}

¹ KAIST Institute for Information Technology Convergence, Korea Advanced Institute of Science and Technology (KAIST), Yuseong-gu, Daejeon 305-701, Republic of Korea#.

² Department of Molecular and Life Science, College of Science and Technology, Hanyang University, Ansan, 15588, Republic of Korea.

³ Department of Cell Modulation, Institute of Molecular Embryology and Genetics, Kumamoto University, Kumamoto, Japan.

⁴ Research Institute for Veterinary Science and BK 21 FOUR program of the College of Veterinary Medicine, Seoul National University, Seoul 08826, Republic of Korea.

⁵ College of Liberal Arts, Hongik University, Seoul, Republic of Korea.

⁶ Korea Atomic Energy Research Institute, 989-111 Daedeok-daero, Yuseong-gu, Daejeon 305-353, Republic of Korea.

* Correspondence: donboscolee@gmail.com (B.-C.L.); kblwhl@gmail.com (K.-B.L.)

Affiliated institution while conducting this research, currently independent

Abstract: Accumulating reports have suggested that an inability to clear dead cells is a cause of inflammation and cancer and that the fascia is associated with cancer metastasis. Novel corpuscle-connected filiform structures (CCFSs) entangled on the fascia of the internal organs of rats were selectively visualized with high repeatability (93%) under vital staining with Janus Green B (JGB). Serial sections of CCFSs stained with haematoxylin and eosin and with Mattson Trichrome were microscopically examined. In parallel, the immunohistochemistry with CD31, Lyve 1, scanning electron microscopy, and transmission electron microscopy (TEM) were also used to investigate the novel properties of the CCFSs. All of the CCFSs enclosed JGB-stained granules, which was verified by the impromptu coupling of stereo and light microscopes and fluorescence-activated cell sorting. The functions of the CCFSs were discovered under fluorescence microscopy and confocal laser scanning microscopy to be implicated in cell death: fragmented DNAs and f-actins with extracellular DNAs. The dead cells in the CCFSs were verified by using terminal deoxynucleotidyl transferase dUTP nick end labelling and TEM. Moreover, the CCFS had a relatively-high concentration of calcium, a main element for cell death in tissue, which was measured in 2-dimensionally images using time-of-flight secondary ion mass spectrometry. Taken these results, we report for the first time that novel reticular CCFSs are widely entangled on the fascia of the internal organs of rats with the implication for cell death.

Keywords: Fascia; cell death; repeatability; immunohistochemistry; Bonghan duct and corpuscle; Janus Green B

1. Introduction

All living bodies organize their lives via homeostasis, in which natural cell death plays a key role as an immune response. In a model of ageing without cell death, at 80 years of age, 2 tons of bone marrow and lymph nodes and a 16-km intestine would be generated in the human body [1,2]. Melino also commented that the rate of cell death was over 20 times faster than that of cell generation by mitosis [1]. However, dying cells are rarely seen in a living body. A review article [3] on cell death coincidentally reported that dead cells were rarely found despite the constant turnover of cells via natural cell death. Moreover, the authors of that review concretely presented the case for such a

curious phenomenon in which even in the thymus, which is where cells die at a high rate, 80% of the thymus did not show any dead cells. Given these observations, where have the many dead cells in living bodies gone?

Despite the mystery of the disappearance of dead cells, new evidence that the failure to clear dead cells could give rise to various pathological conditions, from inflammation to cancer, has emerged [4–6]. A systematic review on the metastasis of ovarian cancers demonstrated that cancer cells under metastasis disseminated to the visceral fascia on the liver and bowel serosa, the omentum, and the mesentery and parietal fascia on the diaphragm [7]. On the other hand, the corresponding anatomical structures through which traditional and alternative medicines exert their effects are closely associated with the fascia system [8,9]. Nevertheless, in modern medicine, the fascia, which consists of collagen and elastin fibres with glycosaminoglycan [10,11], has long been regarded as a supporting matrix for internal organs. However, recent works for biologists and clinicians at a Boston meeting on the fascia system [12] provided some insight into its new role in cancer therapy. Moreover, a current work showed that this intramuscular connective fascia is associated with aging [13].

In the 1960s, a theory for a system of novel anatomical channels, the Bonghan duct (BHD) system, was presented by Kim, Bonghan as the 3rd circulatory system, adding to the blood and the lymphatic circulatory systems [14–16]. Based on experimental data on the BHD system since 2002, Lee and Soh first proposed that the BHD system was closely related with the fascia system, and in 2009, they presented the “Bonghan-Fascia Model” of particular ducts in the fascia system [17]. However, even though the primo vascular system (the new name for the BHD system) has been receiving international recognition, practitioners of orthodox biology and medicine are unfortunately still reluctant to accept the BHD system with fascia, owing to what they consider to be a lack of repeatability.

Thus, for the purpose of scientifically verifying the association of the BHD with the fascia (visceral and parietal) on internal organs in research on cell death, we designed a new vital staining method that stains with Janus Green B (JGB). With this new staining method, we were able, with high repeatability, to reveal corpuscle-connected filiform structures (CCFSs = Bonghan corpuscles and BHD) that were entangled on the visceral fascia (VF) and parietal fascia (PF) of the internal organs of rats. To characterize the CCFSs, we performed diverse examinations: *in situ* and *in vivo* examinations with stereomicroscopy, with serial sections of CCFSs being stained with haematoxylin and eosin using light microscopy and Mattson trichrome staining, with differential immunohistochemistry from lymph and blood vessels, with terminal deoxynucleotidyl transferase dUTP (2'-deoxyuridine 5'-triphosphate) nick end labelling staining, with confocal laser scanning microscopy for whole specimens, with scanning electron microscopy on the CCFSs of the liver serosa and transmission electron microscopy on the CCFSs, with fluorescence-activated cell sorting, and with time-of-flight secondary ion mass spectrometry. From these various investigations, we were able to obtain significant data for the CCFSs that demonstrated their anatomical and histological origins with the implication of cell death within them. Thus, based on these data, we report our finding that CCFSs entangled on the fascia of the internal organs of rats are implicated in cell death and also discuss the potential biological significance of CCFSs.

2. Results

2.1. Anatomical and novel histological characteristics for corpuscle-connected filiform structures (CCFSs)

For the CCFSs on the VF, as shown in Figure 1A, we present the CCFS on the lung of a rat. Under low-magnification stereomicroscopy (SM), we noticed some corpuscular structures (CSs) that were widely scattered on the lung tissue. However, at a higher magnification, we observed filiform structures (FSs) that were connected with the CSs. Some of the FSs were discriminated. However, others were too thin to be resolved under SM. Additionally, for the CCFS on the diaphragm, lower-magnification SM revealed many JGB-stained CSs that were scattered, with some of them being connected to FSs. Under a higher magnification, we determined that the networks of CCFS were present on the outermost connective tissue (PF) of the diaphragm. To demonstrate the relative anatomical geometry of the CCFS, we purposely isolated a CS by using micro forceps, as shown in

Figure 1B. Before elevating the CCFS, it was originally aligned above the blood vessels, as in the inset of Figure 1B. Notably, the blood vessels and fat tissues around the CCFS were not stained.

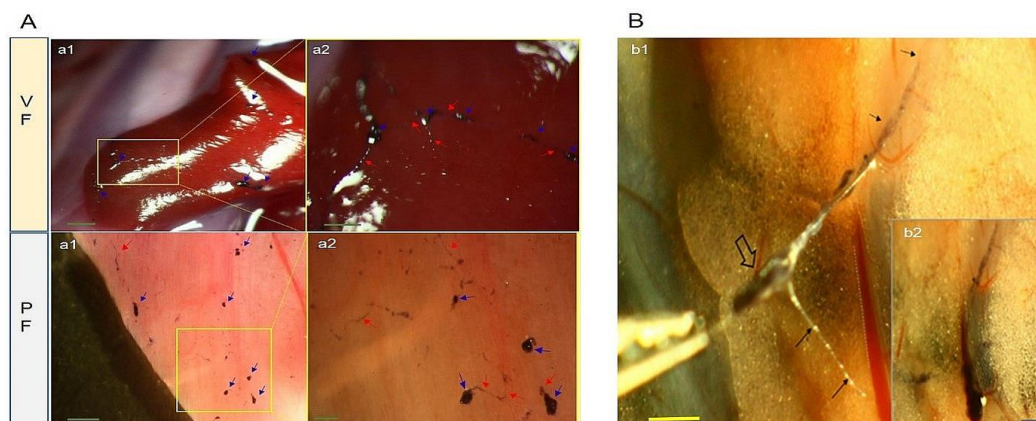


Figure 1. Representative stereoscopic images of the reticular network of corpuscle-connected filiform structures (CCFSs). **(A)** Representative images of the CCFSs on the outermost membranes of internal organs, the visceral fascia (VF), the diaphragm and abdominal walls, the parietal fascia (PF), the VF of the lung, and the PF of the diaphragm are shown. In the VF panel, **a1** indicates a low-magnification view of the CCFSs, in which the blue arrows indicate the corpuscles on the VF of the lung. **a2** shows a magnified view of the yellow rectangle in **a1** where several corpuscle-connected filiform structures are seen, with the locations of the filiform structures and the corpuscles indicated by the red and blue arrows, respectively. In the PF panel, **a1** shows a low-magnification image of the CCFSs, in which most of the CCFSs are (blue arrows) corpuscles that are stained black. However, only one filiform structure connecting the corpuscles, which is indicated by the red arrow, is observed. However, **a2**, which shows a magnified image of the rectangle amid the area in **a1**, distinctively shows several corpuscle-connected (blue arrows) filiform structures (red arrows). Scale bars: in the VF, **a1**: 500 μm and **a2**: 250 μm ; in the PF, **a1**: 500 μm and **b2**: 200 μm . As further demonstrations, some other SMs of the CCFSs are uploaded in the Figures S10, S11, and S12). **(B)** In situ *and* in vivo direct holding technique: CCFSs slightly elevated using micro forceps. The arrows indicate the CCFS (**b1**) on the VF of fat tissue around the vena cava in a deep area of the abdomen. The open arrow points to a corpuscle that is heavily stained with JGB. Notably, the blood vessel beneath the filiform structures is not stained. The inset (**b2**) shows an original image of the CCFS before it was lifted with micro forceps. Both scale bars are 500 μm .

To verify the existence of novel CCFSs entangled on the VF and PF, we examined the CCFSs on the small intestine (VF) and those on the diaphragm (PF), respectively, using impromptu coupling on site, and the results are shown in Figure 2. Under low magnification, stereomicroscopy (SM) of the small intestine showed dark CCFSs scattered on the reddish-coloured surface (VF) of the small intestine. The exact morphology of a CCFS can be barely recognized under this low of a magnification, and clearly, the FSs are not seen. However, once a small area (dotted rectangle of a1 in Figure 2) was magnified, we were able to obtain a clear view of the CCFS with an FS on the small intestine in situ and in vivo. Immediately after such an SM observation, we partially isolated the visualized area, a1, of the VF, and made an LM preparation. Thus, we were able to directly compare the in situ and in vivo images of the CCFSs on the small intestine with their in vitro LM images. Thus, the image of the CCFS in the dotted rectangle (a1 of the VF) corresponds exactly to the LM image of the CCFS (a3 of the VF). The LM image of the CCFS shows distinctive CCFS features with corpuscular and filiform structures connected, demonstrating that both of them are composed of JGB-stained granular structures.

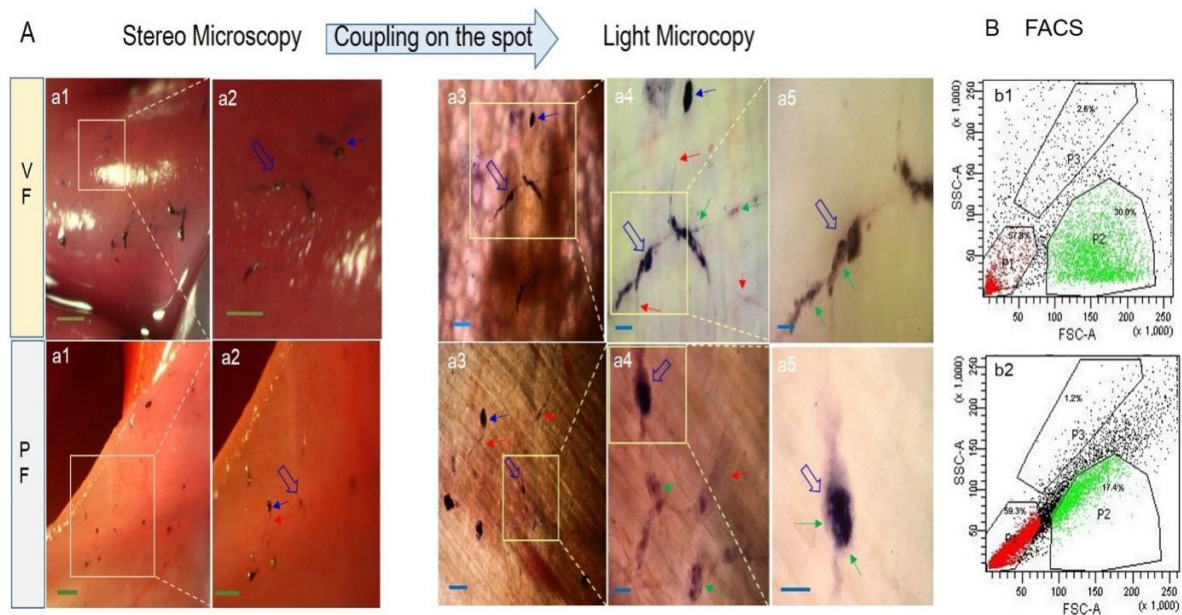


Figure 2. Impromptu coupling examination using stereomicroscopy and light microscopy of corpuscle-connected filiform structures (CCFSs) on the small intestine (visceral fascia, VF) and diaphragm (parietal fascia, PF), as well as fluorescence-activated cell sorting (FACS). (A) The VF panel shows stereoscopic images (SMs) of CCFSs on the serosa membrane of the small intestine. (a1) Low-magnification SM for the distribution of CCFSs visualized on the small intestine. Among the blackish CCFSs in a1, the area inside the dotted rectangle is magnified, and the image is shown in a2. The corpuscles are distinctively visualized. The corpuscles in a2 are clearly revealed in vitro under a light microscope (a3, a4 and a5). The rectangle in a3 is magnified into a4, where the filiform structures (red arrows) between the corpuscles (blue arrows) are clearly visualized. At this magnification, a4, the JGB-stained granules (green arrows) are noticed. The granules (green arrows) are revealed in a5. Scale bars: a1: 500 μm ; a2: 150 μm ; a3: 100 μm ; a4: 50 μm ; and a5: 50 μm . The PF panel shows the SMs of CCFSs on the outermost membrane (PF) covering the diaphragm. (a1) Low-magnification SM for the distribution of CCFSs on the diaphragm of a rat is shown. The rectangle in a1 is magnified into a2, in which corpuscles (blue arrows) are clearly revealed with some filiform structures (red arrows). The SMs of a2 are clearly visualized in vitro under a light microscope (a3, a4 and a5). The rectangle of a3 is magnified into a4, in which filiform structures (red arrows) between corpuscles (blue arrows) are revealed by the JGB-stained granules (green arrows). Many of the granules (green arrows) are clustered into a corpuscle in a5. Scale bars: in the VF, a1: 500 μm and a2: 500 μm ; in the PF, a3: 200 μm , a4: 50 μm , and a5: 50 μm . (B) Distributions of the components of the CCFSs (b1) and controls (b2) via FACS. In (b1), the P1, P2, and P3 are 57.3%, 30% and 26%, respectively, and in (b2), they are 59.3%, 17.4% and 12%, respectively. The x-axis: FSC-A and y-axis: SSC-A represent the relative sizes of the components (cells and granules, respectively) and their granularities.

As shown in the PF panel of Figure 2, visualized in situ and in vivo CCFSs were, at first, examined under SM (a1 and a2). Then, the SM images of the CCFSs were coupled with the light microscopy (LM) images from a2 to a3, a4 and a5, as indicated by the arrows. The images in a2 ~ a5 show that the CCFSs are composed of JGB-stained granules, which could be attributed to the novel filiform and corpuscular structures. As shown in B of Figure 2, the significant difference between a CCFS and control tissue is that the CCFS shows a high granularity with components of various sizes.

Next, we applied scanning electron microscopy (SEM) to determine how the CCFSs were distributed on the internal organs of a rat (Figure 3). For that purpose, with the abovementioned coupling method, we first observed the CCFSs on the liver of a rat under LM immediately from the stereoscopic findings shown in a1 and a2. These LM images of CCFSs on the liver showed that some CSs were present (a1). Even though the images clearly revealed CSs, clear FSs could be barely seen. However, magnified LM images (a2) demonstrated that not only FSs but also hidden CSs were

present. After this first step, we examined the CCFS on the liver under SEM. Successive magnifications of the SEM images of the CCFS (b1 to b7) demonstrated that the CCFS was entangled not only on the serous VF but also in the loose connective fibres of the VF. An SEM image of the CCFS revealed that all of the CSs were connected with an FS, which could not be discerned under LM.

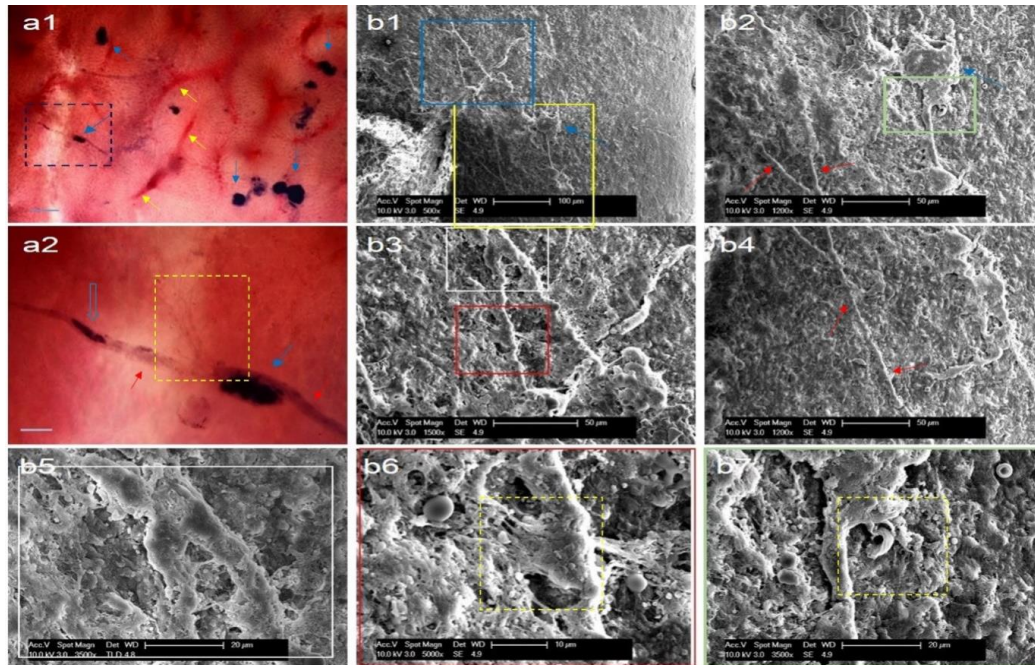


Figure 3. Scanning electron microscopy (SEM) images (**b1 ~ b7**) of the corpuscle-connected filiform structures (CCFSs) on the outermost membrane, the serous visceral fascia (VF), of the liver based on light microscopy images (LM, **a1**, and **a2**). In **a1**, some CCFSs (blue arrows) are visualized on the liver; the CCFS in the rectangle is magnified into **a2**. In **a2**, two corpuscles (two blue arrows) are seen with distinctive filiform structures (red arrows). However, the open blue arrow indicates a small corpuscle, which is not seen in **a1**. The yellow dotted rectangle in **a2** shows the CCFS entangled with the outermost membrane of the liver, which shows the same pattern as those in the SEM images (yellow-dotted rectangles) in **b6** and **b7**. Scale bars: **a1**: 100 μm and **a2**: 50 μm . Under SEM, **b1** shows the lowest magnification image of a CCFS on the liver. The blue rectangle in **b1** was magnified into **b3**. The yellow one in **b1** was magnified into **b2** and **b4**, where the blue arrow indicates the same corpuscle. Clear filiform structures (red arrows) are revealed in **b2** and **b4**. The white and red rectangles in **b3** are magnified into **b5** and **b6**, respectively. The green rectangle in **b2** is magnified into **b7**. Notably, the images of the CCFSs (yellow dotted rectangles) in **b6** and **b7** show that they are entangled on the outermost membranes, the serosa, of the liver, as shown in the yellow-dotted rectangle in **a2**.

To obtain the histological characteristics of the CCFSs, we observed the CCFSs after staining them with haematoxylin-eosin (HE) and Masson Trichrome (MT) staining. HE staining of the CCFSs on the small intestine revealed that it was located on and embedded in the outermost membrane, the serous VF, of the small intestine. Histologically, the CCFSs showed a more basophilic makeup than the serous membrane. Noticeably, at 1,000 \times magnification, the CCFSs were seen to contain basophilic granules with pale-coloured cytoplasm cells. Figure 4 shows the images of serially cut HE-stained and MT-stained CCFSs in numerical order. Similarly, to the images of the HE-stained CCFSs, the images of the MT-stained CCFSs showed that they were floating on and/or embedded in the small intestine. In addition, the images of the MT-stained CCFSs showed that they consisted of different fibres, with the outermost fibres being blue-coloured collagen, which is a hallmark for the outermost serous membrane of visceral organs.

On serial sections of the same specimens stained with HE or MT, we performed immunohistochemical staining to differentiate the CCFSs from lymphatic and blood vessels. For this

work, we used a lymphatic endothelial maker, LYVE-1, and a blood vessel endothelial marker, CD31. As shown in Figure 4C, lymphatic and blood vessels were positive to LYVE-1 and positive to CD31, respectively. However, the CCFs on the small intestine were negative to both antibodies but with different colours.

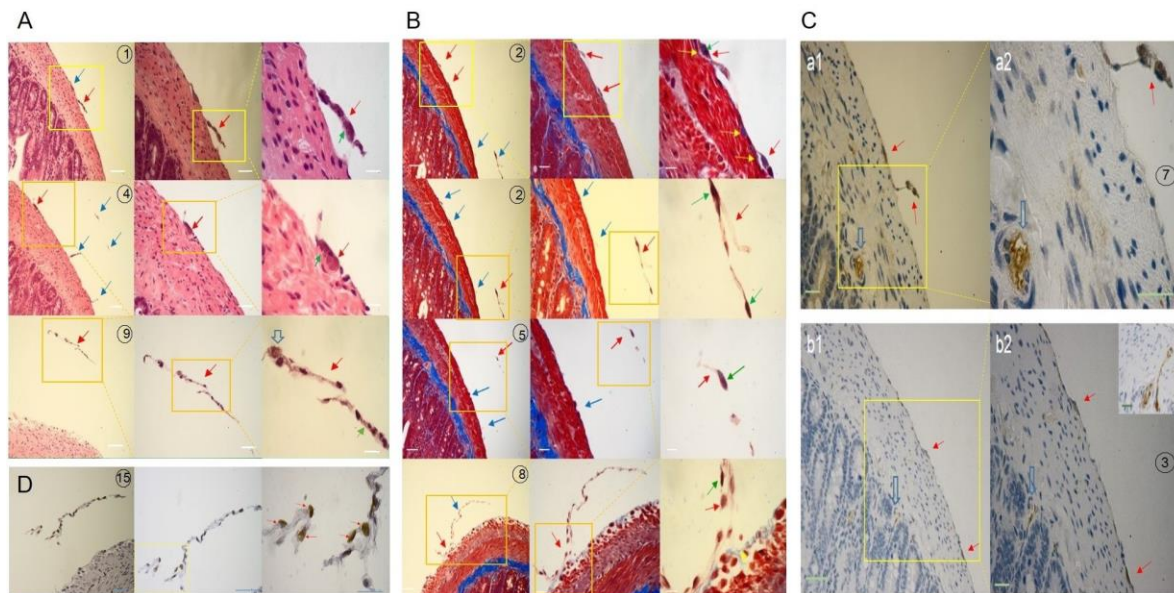


Figure 4. Histological characteristics of corpuscle-connected filiform structures (CCFSs) on the outermost membrane of the serially sectioned small intestine. Each number shows a gradual magnification (200', 400' and 1,000') of the same specimen from left to right in **A**, **B** and **D**. For **C**, two magnifications, 200' and 400', are seen. (**A**) Haematoxylin and eosin staining. The blue arrows show nearby CCFs in the same area with the filiform structure (FS), which is indicated by the red arrow. In the magnified view of the CCFS (1000'), basophilic granules (green arrows) and a pale cytoplasmic cell (open arrow) are observed. Scale bars: 50 μm (200'), 40 μm (400'), and 10 μm (1,000'). (**B**) Mattson trichrome staining. The red arrows indicate the CCFs, and the blue arrows show other nearby CCFs in the same area as the FS, which is indicated by the red arrow. Image number 2 is divided into two parts in both the upper and lower panels. Notably, in the magnified (1000') view of the CCFS in slide number 8, some outermost blue-coloured collagen fibres (yellow arrows) and heavily stained nuclei (green arrows) with thin-sectioned white-brown FS are observed. Scale bars: 50 μm (200'), 40 μm (400'), and 10 μm (1,000'). (**C**) Immunohistochemistry with LYVE-1 (**a1**, **a2**) and CD31 (**b1**, **b2**). The lymphatic vessel (open blue arrow) was stained in a bright brown colour using LYVE-1. However, the CCFS (red arrow) was negative against LYVE-1, as shown by the dark grey colour with blue. For the CD31 staining, the CCFs (red arrows) were stained in dark grey. However, the blood vessels (open arrow and inset) show a bright brown colour. Scale bars: **a1**: 20 μm (200'), **a2**: 20 μm (400'), **b1**: 40 μm (200'), **b2**: 20 μm (400'), and inset: 20 μm (200'). (**D**) Terminal deoxynucleotidyl transferase dUTP nick end labelling (TUNEL). The cells positive against TUNEL, the dead cells, are seen at 1000' magnification (red arrows). However, the cells negative against TUNEL, the live cells, are seen as blue-coloured ones. Scale bars: 50 μm (200'), 40 μm (400') and 10 μm (1,000').

2.2. The implication for cell death in the CCFs

For this work, we used the terminal deoxynucleotidyl transferase dUTP nick end labelling (TUNEL) staining method, as it has been used as a cell death marker by indicating apoptotic cells among tissues. The images in Figure 4D clearly show dead cells, which account for approximately half of the cell population in the CCFs, with live cells being blue due to counter staining with Mayer's haematoxylin.

With these pieces of histological evidence, under light microscopy and fluorescence microscopy, we examined the CCFs isolated from the large intestine and the abdominal wall of rats as representative CCFs of the visceral and parietal fascia, respectively, and the results are shown in

Figure 5. For this work, we stained the pure CCFSs using 4', 6-diamidino-2-phenylindole (DAPI) for DNA molecules and phalloidin for F-actin molecules. Overall, the microscopic images showed that the CCFSs consisted of CSs and their connected FSs, all of which were visualized due to the JGB-stained granules. These granules were seen distinctively under bright-field LM and were not stained with DAPI (Figure S1). Notably, for the F-actin molecules in the CCFSs, many fragmented F-actin signals, as shown in a3 of Figure 5, were seen. Clearer images of the fragmented F-actin molecules were obtained using confocal laser-scanning microscopy (CLSM), and the results are presented in b9 and b10 of Figure 5. Another indication of the presence of dead cells came from the images of the DAPI-stained DNA: the FM and CLSM images of randomly distributed threadlike extracellular DNA molecules on the CCFSs are shown in a5 and in b11 and b12 of Figure 5, respectively. One more notable fact is that the CCFSs contained DNA fragments that had been stained with DAPI, as shown in a5 of Figure 5. The fragmented DNA molecules were only slightly discernible in the FM images. However, digital magnification was helpful for recognizing the DNA signals associated with the fragmented DNA. Images of eDNA, fragmented F-actin molecules, and granular fragmented DNA are pieces of significant evidence implying that CCFS consists of dead cells. We also uploaded other clear FM and CLSM images to prove the existence of distinctive eDNA molecules, fragmented F-actin molecules, and granules of fragmented DNA molecules in CCFSs (Figures S2–S5).

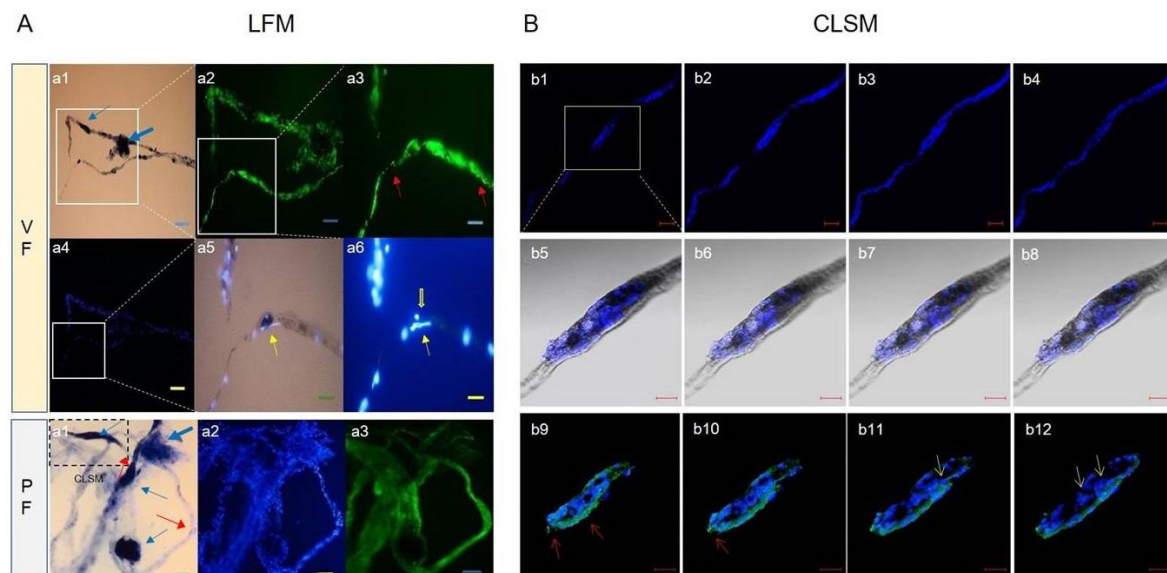


Figure 5. Light and fluorescence microscope (LFM, **A**) and confocal laser scanning microscopy (CLSM, **B**) images of isolated corpuscle-connected filiform structures (CCFSs). (**A**) For the visceral fascia (VF), **a1** is a light microscopy (LM) image of a CCFS in which clear corpuscles (blue arrows) with filiform structures (red arrows) are seen. The rectangle in **a1** is magnified into **a2** with F-actin (green colour). The rectangle in **a2** is magnified into **a3** with fragmented F-actins (red arrows). The DAPI image of **a4** corresponds to the LM image shown in **a1**. The rectangle in **a4** is magnified into **a5**, which shows a merged image between the DAPI and the bright-field images. In **a5**, the yellow arrow indicates extracellular DNA (eDNA) on a JGB-stained corpuscle. The DAPI image in **a6** shows weakly dotted signals for DNA (original raw data: Figure S6). In the parietal fascia (PF), **a1** is a merged image of the light and the DAPI images of a CCFS in which the four blue arrows indicate corpuscular structures. Between the corpuscles are FSs (red arrows). **a2** and **a3** present an image of the DAPI-stained CCFS and an image of the F-actin in the CCFS, respectively. Scale bars: in the VF, **a1**: 100 μm , **a2**: 50 μm , **a3**: 25 μm , **a4**: 100 μm , **a5**: 25 μm , and **a6**: 25 μm ; in the PF, **a1**, **a2** and **a3**: 40 μm . (**B**) CLSM images of the CCFS stained using DAPI optically sectioned by 2 μm and arranged from **b1** to **b4** in 12- μm intervals. Rod-shaped nuclei are arranged in the rectangular portion (corpuscle), which is magnified and optically sectioned (by 1 μm) into **b5** to **b8** (6- μm intervals). The yellow arrows in **b5** to **b8** show JGB-stained granules, not DAPI-stained granules. The images from **b9** to **b12** show fragmented F-actin molecules (red arrows) with DAPI-stained DNA molecules. These were also

optically sectioned by 1 μm and arranged in 6- μm intervals. eDNA images (yellow arrows) are noticed. CLSM images for fragmented DNA and F-actin are uploaded as Figures S3–S5. Scale bars: **b1** ~ **b4**: 50 μm , **b5** ~ **b8**: 20 μm , and **b9** ~ **b12**: 20 μm .

To identify the elements contained in the CCFs, we applied time-of-flight secondary ion mass spectrometry (TOF-SIMS) to the CCFs. The specimens for TOF-SIMS (Figure 6) and TEM (Figure 7) were taken from the abdominal wall, as shown in the SM of Figure 7. TOF-SIMS examination of the CCFs provided information on the components of the CCFs, as well as morphological data, as shown in Figure 6. Calcium and oxygen were identified as being the major elements in the cations and anions of the CCFs, respectively. The images in Figure 6 were selected from among all the data in order to determine the overall major elements, generally those related to the living body. All the data obtained for the CCFs via TOF-SIMS were uploaded and are shown in Figures S6 and S7.

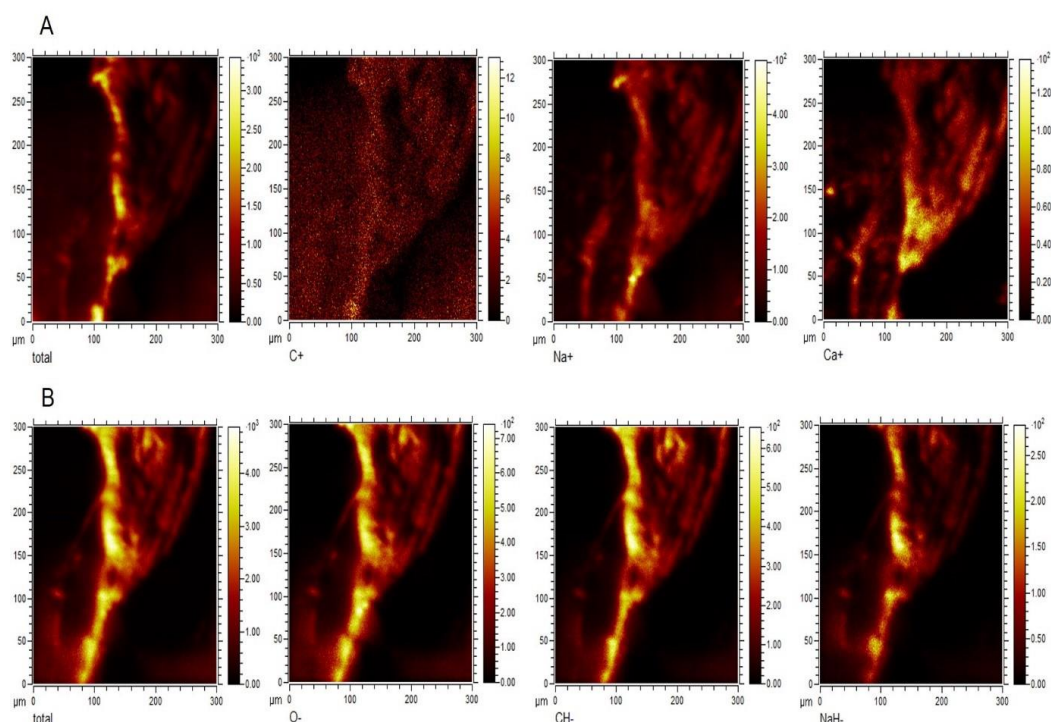


Figure 6. The distribution of major elements in the corpuscle-connected filiform structure (CCFS) (2D) image 2-dimensionally d by time-of-flight secondary ion mass spectrometry (TOF-SIMS). The x-axis and y-axis show a 300 μm \times 300 μm area of the CCFS scanned by using TOF-SIMS, and each coloured bar indicates the relative concentration of the element. (A) 2D images for the major cations (C, Na, and Ca) in the CCFS and the total image of the CCFS. (B) 2D image for the major anions (O, CH, and NaH) in the CCFS and the total image of the CCFS. The most abundant elements in the cations and anions of CCFS are silicone and oxygen molecules, respectively. Additionally, a relatively high concentration of calcium ions is present in the cations of the CCFS. However, single carbon molecules are rarely seen. The raw data are uploaded in Figure S7.

More information on the CCFs was obtained from TEM examination, and the results are shown in Figure 7. For this, we examined the CCFs on the abdominal wall of a rat. Among several CCFs, we isolated some, as indicated by the dotted rectangle in 'a' for the TEM process. The lowest magnification image of FSs is shown in b1, from which two parts (b2 and b3) were obtained as magnified images of b1. The FSs, as seen under TEM, are surrounded by the outermost membrane inside which many confluent vacuoles with fibrous structures are seen. Dead cells are observed in the CSs, showing the moment when the cell membrane disintegrates, the nucleolus is disintegrated, and the cytoplasm becomes transparent. Around these cells, many granules of varying size are seen.

Intriguingly, we observed bone marrow-derived polychromatic erythroblast-like cells with normal red blood cells in the CS with dead cells.

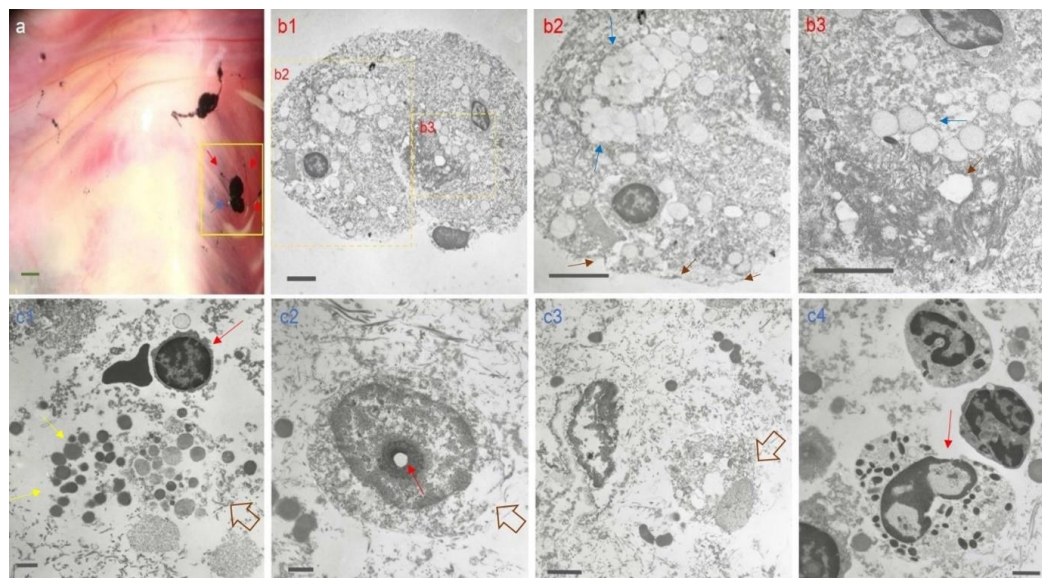


Figure 7. Transmission electron microscopy (TEM) images of corpuscle-connected filiform structures (CCFSs). The 'a' picture is a stereoscopic image immediately after visualization of CCFs on the abdominal wall of a rat. Among the CCFs in 'a', we took the CCFs in the yellow rectangle for TEM examination. The filiform structures (red arrows) examined via TEM are presented as cross-sectioned images in **b1**, **b2** and **b3**. In **b1**, a filiform structure with a roundish shape is seen. The yellow rectangles in **b1** were magnified into **b2** and **b3**, respectively. In **b2**, confluent vacuoles (blue arrows) were seen inside the outermost membrane, which is indicated by three dark brown arrows. In **b3**, a clear pore surrounded by fibrous structures (dark brown arrows) and confluent vacuoles (blue arrows) are seen. The images (**c1** ~ **c4**) shown in the second panel were obtained from a TEM examination of the corpuscle (blue arrow) in the stereoscopic image in 'a'. In **c1**, many granules (yellow arrows) from a completely disintegrated cell (open arrow) are seen. In **c2**, a disintegrated nucleolus (red arrow) and a disrupted cytoplasmic membrane (open arrow) are seen. The image in **c3** shows translucent cytoplasm with pores (open arrow). The **c4** image shows the moment of cell disintegration from the cytoplasmic membrane (red arrow). Among the TEM images of the corpuscle in **c1**, a polychromatic erythroblast-like cell (red arrow) with erythrocytes was detected. Scale bars: **a**: 500 μm ; **b1**, **b2**, and **b3**: 5 μm ; **c1** and **c2**: 1 μm ; **c3**: 2 μm ; **c4**: 1 μm .

2.3. Statistical data for CCFs and their existing tissues

For this work, we sacrificed 15 rats, 14 of which showed CCFs that could be visualized (93%) using this method. The visualized CCFs and their associated internal organs are summarized in Table S1. To understand the overall distribution of the CCFs, we summarized the sizes of the biggest and smallest CSs in each tissue where the CCFs were found. Moreover, the distance between two CSs (the most distinctive CSs in a CCFs under SM) was added into the table. The criterion for the data on the numbers of CSs in Table S1 depended on how distinct the SM image was. Thus, the possibility that more CSs may have actually been present in the image than could be counted exists. According to Table 1, the CSs were most frequently found on the liver (138), followed by the abdominal wall (114), the small intestine (112), fat tissue (57), the mesentery (45), the large intestine (17), the epididymis (12), the lung (12), the diaphragm (10), the ovary (10), the parietal pleura (6), and the testis (5).

3. Discussion

Using staining with Janus Green B (JGB), we were able to visualize reticular CCFSs entangled on the fascia system covering internal organs in the peritoneal and thoracic cavities of rats with high repeatability, and to the best of our knowledge, this is the first time that this has been done. The anatomical and histological novelties of these CCFSs were identified through imaging studies. Concomitant with such novel characteristics, the CCFSs in different fascia of internal organs shared a common characteristic, i.e., the envelopment of JGB-stained granules inside them. We have also found that the CCFSs were closely implicated in cell death using diverse microscopic investigations and TOF-SIMS.

The above mentioned findings reminded us of the mysterious work by Bonghan Kim in the 1960s (Figure S8), in which he had insisted that the network system on the internal organs is part of a 3rd circulatory system that is independent of the cardiovascular and the lymphatic systems [14–16]. Since Kim's report, several articles have been published describing the mysterious structures, which are named Bonghan ducts (BHDs) and Bonghan corpuscles (BHCs), on internal organs that had been identified using various methods [18–21]. When comparing our new findings with those in the articles, we recognized that the previous articles could be classified into two categories based on the sampling procedure. The first category is based on Fujiwara's work in the 1970s, which was research on Bonghan Kim's original claim (Fujiwara and Yu 1967). Based on Fujiwara's approach, the first result from Soh's team on the mysterious structures on the internal organs of rabbits was produced in 2005 [18]. The second category is based on the chemical dyes used to visualize the new anatomical structures on the internal organs of animals [23,24].

Even though some findings imply the existence of such new anatomical structures on the internal organs, skepticism has remained in the major sciences, which is mainly owed to the lack of scientific repeatability. Moreover, we found that one of the most important limitations in previous works was the lack of a heparinized condition before the visualization was performed. So that we would be able to specifically visualize only the CCFSs, we removed even the slightest chance of blood clotting by treatment with heparin via intravenous injection and intraperitoneal injection. In one rat among the 15 rats, we failed to visualize the CCFS clearly enough to provide statistical data. This was probably the result of us using a low concentration of JGB with a short peritoneal incubation. However, as summarized in Table S1, with high repeatability (93%), we were able to visualize CCFSs on various internal organs. They were specifically revealed in the loose connective tissues and fascia, covering internal organs in the peritoneal and thoracic cavities of rats.

More importantly, in order to realistically and immediately verify the existence of CCFS without further examination, we developed an impromptu coupling method to compare the SM and LM of the same CCFS on an internal organ, such as the intestine or the diaphragm (Figure 2). This impromptu coupling of the SM and LM for the same specimen made possible a connection between the CCFS revealed in the SM and that revealed in the LM of the JGB-stained granules in the CCFS. This direct comparison allowed us to be certain that novel anatomical structures were entangled on the fascia of internal organs before we conducted further examinations. By using this coupling method, we found that the CCFSs had a reticular form and were as dense as nearby blood capillaries on the same tissue, as shown in Figures 1 and 2. Such findings suggest that CCFSs are novel anatomical structures distinctly different from those previously reported on the same internal organs. In addition, we recognized that owing to the fluorescence ($\lambda_{\text{max}} = 660 \text{ nm}$) of JGB [25], the JGB-stained structures in the CCFSs could be sorted and distributed, as shown in Figure 2. Their distributions were different from those of the control tissue in terms of granularity and relative size, indicating that the CCFSs and nearby control tissues were different not only in morphology but also in content. Moreover, the widely scattered distribution in the test CCFS compared with that in control tissue implies that CCFSs consist of many disintegrating cells, as well as normal cells.

Thus, by coupling the results of the SM and LM examinations with pilot FACS data for JGB-stained structures, we postulate that the reason JGB incubation selectively revealed the CCFSs may be JGB's selective staining target in the granules of the CCFSs. Unfortunately, with these FACS data, we were unable to correlate the distributions and images in all of the areas, P1–P3, of the CCFS via a re-collection

process. However, in future work, this FACS approach using the auto fluorescence of JGB-stained granules will play an important role in developing specific markers or antibodies for the CCFSs.

JGB molecules were first reported by Michaelis for supra vital staining of mitochondria [26]. However, as a vital staining dye in living bodies, Yack first used JGB to visualize nerves [27]. However, its binding to sites in the nervous system was not clear enough for further application. Furthermore, Lee et al. injected JGB dissolved in ethyl alcohol into the lymphatic vessels of rabbits for visualization of the BHDs and BHCs. However, the solvent for JGB, ethanol, turned out to be harmful to the inner walls of the lymphatic vessels [28]. Lazaro and Cooperstein described the specific proteins in the mitochondria that might be the binding sites for JGB molecules [29]. However, the target molecules in the mitochondria or nerves that are stained by JGB still require investigation. Thus, even though JGB incubation could specifically reveal the novel CCFSs on the internal organs of rats, as shown in our data, the precise mechanism for JGB's ability to preferentially stain the novel anatomical structures, CCFSs, *in situ* and *in vivo* needs to be elucidated.

Based on these results, we can summarize the biological characteristics of the CCFSs as follows: a CCFS reticular network entangled on the fascia of internal organs (Figures 1–3), a differential immunohistochemistry different from those of lymph and blood vessels (Figure 4C), the presence of dead cells, as revealed by TUNEL staining (Figure 4D), and the co-existence of approximately 1- μ m-sized DNA particles, extracellular DNA signals (DAPI), and signals for fragmented F-actin in the CCFSs (Figure 5), a comparatively high 2D concentration of calcium ions in the CCFSs, as determined using TOF-SIMS (Figure 6), and the presences of disintegrating cells, many cytoplasmic vacuoles, and ruptured plasma membranes, as shown in the TEM images (Figure 7).

Under apoptosis, DNA fragmentation and blebbing of plasma membranes and apoptotic bodies are observed, and fragmented actin molecules play a key role in apoptosis of cancer cells [30]. Choi et al. reported that eDNA was released *in vitro* via apoptosis and necrosis in cells [31]. In ophthalmology, eDNA was also investigated, and the images of DAPI-stained eDNA were unique [32], which is in agreement with our eDNA images. Moreover, TUNEL has been widely used for detecting fragmented DNA molecules by labelling the 3'-hydroxyl terminals in double-stranded DNA molecules broken under apoptosis [33]. Notably, according to recent applications of TOF-SIMS to biological tissues, a relatively high concentration of calcium in a tissue is thought to be an indication of dying cells [34]. And at present we do not understand why the concentration of oxygen in CCFSs is relatively higher than that of other anion elements. However, we pay attention to the role of oxygen in regeneration, stem cell and cell death as some works reported on the role of oxygen for wound healing [35], neural stem cells and apoptosis [36]. The TEM images in this study provided evidence for the existence of dead cells. Thus, a summary of the biological characteristics for CCFSs, as found in this study, leads to the conclusion that cell death is associated with the physiological functions of the CCFSs among the internal organs.

The first concept of natural cell death has its basis in Kerr et al.'s "apoptosis," which was published in 1972 [37]. In general, cell death in living bodies can be understood by two main streams, apoptosis and necrosis [38]. Between these two types, we hypothesize that CCFSs may contain necrosis-like cells based on the above necrosis characteristics, many vacuoles, ruptured plasma membranes, and disintegrating cells, which were found in this study. Furthermore, given that dead cell-containing CCFSs were *in situ* and *in vivo* visualized without damaging serous membranes near the CCFSs, as shown using TUNEL staining (Figure 4), the process of cell death in the CCFSs might be very specific in terms of anatomical location. Recent data have shown that this TUNEL process could stain not only apoptotic dead cells but also necroptosis-evoked dead cells, which are necrosis-like but are programmed for cell death [39].

TEM has been used to clearly describe the morphological characteristics of dead cells. In TEM images showing apoptosis and necroptosis, apoptotic cell death is characterized by a condensed cytosol, marginalized chromatin, and fragmented nuclei. However, the characteristics of necroptosis are a permeabilized plasma membrane and the translucence of the cytoplasm [40]. As shown in Figure 7, TEM images of the CCFSs showed necroptosis-like features such as ruptured plasma membranes with granules and cytoplasmic translucence. Based on these TEM images and the

TUNEL-positive images, we conjecture that cell death in the CCFs may resemble a naturally programmed necrosis, named “necroptosis,” rather than only necrosis. However, these TEM images did not show every kind of dead cell in the CCFs. Recently, cross-talk among different types of cell death, apoptosis, autophagy, necrosis and necroptosis, have been reported [41,42]. Based on the data with implications of cell death in the CCFs, we assume that these novel CCFs could be venues for dynamic cell death with cross-talk depending on the physiological and pathologic conditions. Furthermore, given that the CCFs are widely and densely located in the loose connective tissue of the fascia system, as shown in our results, the CCFs may serve as hiding places for dead cells, possibly answering the question as to where the numerous dead cells in living bodies have gone [1–3].

On the other hand, medical evidence that a lack of the clearance of dead cells in a living body could be a trigger for tissue inflammation and cancer has been accumulating [4–6]. The specific genes and proteins that modulate cell death as signals have been investigated [43,44]. In addition to such molecular approaches, alternative and comprehensive applications have been considered in order to reduce cancerous symptoms via modulating the fascia system. For example, Langevin and colleagues insisted that cancer patients, as well as many others, might be helped by a proper manipulation of the connective tissues of the fascia system [45]. However, basic studies that explain the clinical effects of the fascia systems in the treatment of patients with cancer have been too limited to determine the role of the connective fascia tissues in ameliorating cancerous clinical findings. Nonetheless, a systematic review on the metastasis of ovarian cancers in the peritoneal cavities made clear that the pattern for the metastasis of cancer cells was closely related with the fascia systems [7]. Even in 1964, a clinical study involving 500 patients showed that the removal of the fascia causes more frequent metastases of malignant skin melanomas [46]. Such reviews and clinical studies on the fascia and metastasis have given us insight into the close inter-relationship between the therapeutic role of the fascia in clinics and the pattern of cancer metastasis with the fascia.

4. Materials and Methods

4.1. Experimental animals

For this work, we used rats (Wistar rats; 8 females and 6 males, 150~250 g) that were kept in a well-ventilated room before the start of the main experiment, in accordance with international guidelines under approved protocols. For general deep anaesthesia, we used inhalation anaesthetics, i.e., halothane-related anaesthetics such as ethers, with an adjunctive intramuscular injection of urethane (1.5 g/kg) when necessary. All of the experiments were approved by the animal committee of the Korea Advanced Institute of Science and Technology (KAIST).

4.2. Visualizing steps for Corpuscle-connected filiform structures (CCFs) on the internal organs

As a visualizing dye, we used Janus Green B (Sigma, JGB) dissolved in phosphate buffered saline (pH 7.4, PBS) or sterilized saline, and we adjusted the volume of the solution so that the concentration of JGB was 0.1%. Next, we filtered the dissolved JGB via 0.45- μ m pore size membrane filters. The filtered 0.1% JGB was kept in an incubator at 37~38°C before the application. The 0.1% JGB was prepared with 10 U of heparin (Sigma) solution (10:1 (v/v)). Before the visualization, we injected approximately 0.2~0.4 ml of the heparin solution (10 U in PBS) into the femoral vein. Then, for the visualization of the CCFs, we injected approximately 0.8 ml~1 ml of JGB with heparin (10:1) into the peritoneal cavities of the rats, which were under deep anaesthesia. An incubation time of 30 min to 1 h was found to be proper for the best visualization of the CCFs on the internal organs of the rats. In rare cases, we injected the dye solution, approximately 0.2 ml, into the thoracic cavities of the rats after the experiments involving their peritoneal cavities had been completed. As soon as possible after the experiments, we euthanized the rats by causing them to inhale ether.

4.3. Stereoscopic observation of CCFSs on the internal organs in situ and in vivo

After the vital staining with JGB for 30 min to 60 min in the peritoneal and thoracic cavities, we first opened the abdomens of the rats by cutting the medial alba to not make them bleed. Immediately after exposing the internal organs, in some cases, we slowly added warm saline into the abdominal cavity to wash out the overloaded JGB. After that, under a stereomicroscope (STX 60X, Olympus, Japan), we observed the CCFSs on the fasciae of the rat's internal organs, which were specifically well-stained by JGB as a dark blue to black colour.

4.4. Impromptu coupling method of stereomicroscopy (SM) and light microscopy (LM) on the same visualized CCFS on internal organs

After euthanasia, we observed the CCFSs on the internal organs in situ and in vivo under a stereomicroscope. Immediately after that, we partially cut the fixed CCFS containing the internal organ, which we mounted using DAPI with anti-fading agents (Thermo Fisher Scientific, USA). Impromptu and on site, the specimens were examined using a light microscope (BX53, Olympus, Japan) with a CCD camera (eXcope X3, DIX, Korea). The images obtained using LM and SM were compared.

4.5. Following methods are applied by using general sample preparation

Fluorescence-activated cell sorting (FACS). Sample preparation for histology of the CCFS in the small intestine. Staining of the CCFS with haematoxylin and eosin (HE) and Masson Trichrome (MT). Terminal deoxynucleotidyl transferase (TdT) dUTP nick end labelling (TUNEL) staining. Immunohistochemistry for characterization of CCFS. Fluorescence microscopy (FM) and confocal laser scanning microscopy (CLSM) imaging of an entire pure CCFS. Scanning electron microscopy (SEM) of the CCFS on the liver. Time-of-flight secondary ion mass spectrometry (TOF-SIMS). Transmission electron microscopy (TEM) of CCFSs.

5. Limitation and Further Studies

For reproducibility in other labs we present still and movie images of visualized corpuscle-connected filiform structures (CCFSs) (Figure S9, Video S1) and address one critical limitation: this staining method could not be used in visualizing the whole network of the novel CCFSs in a single experiment. To reveal the whole system for CCFSs, several experiments should be carried out as fascia systems covering internal organs are distributed in a complex. Beyond this limitation, two important further studies remain; one is to find antibodies and aptamers selectively binding to CCFSs, and another is to develop an optical device free from chemical staining to reveal CCFSs for clinical application.

6. Conclusions

With high repeatability by using Janus Green B vital staining, we presented the evidence that novel reticular corpuscle-connected filiform structures (CCFSs) are widely entangled on the fascia of the internal organs of rats with the implication for cell death. Under basic and clinical trends of the fascia system, we hope that our newly found CCFSs, along with modern therapeutics for such cell death-related diseases as inflammation and cancers, might play beneficial roles in further studies.

7. Patents

This work was patented in Korea (Korean Patent: 1021510880000).

Supplementary Materials: The following supporting information can be downloaded at the website of this paper posted on Preprints.org.

Author Contributions: K.-B.L., B.-C.L., and H.G.K., development of Janus Green B staining method, conceptualization; B.-C.L., samples collection, histological examination, time-of-flight secondary ion mass

spectrometry, fluorescence-activated cell sorting, image analysis and data statistics, draft of manuscript, review and editing; J.Y.L., confocal scanning microscopy, Scanning electron microscopy; K.-S.L., transmission electron microscopy, review and editing; I.L., histological examination, immunohistochemistry, review and editing; H.G.K., critical revision of the work, review and editing; K.-B.L., supervision. All authors have read and agreed to the published version of the manuscript.

Funding: This work was carried out as a contract research project presented by Korea Atomic Energy Research Institute (79101-16). We appreciate Hyung Guhn Park, Jin Soo Ko and the National Research Foundation (NRF) of Korea funded by the Ministry of Education, Science, and Technology (NRF 2016-R1D1A1A09919546) for their financial support.

Institutional Review Board Statement: The study was conducted in accordance with the Declaration of Helsinki, and approved by the Institutional Review Board of KAIST.

Informed Consent Statement: Not applicable.

Data Availability Statement: Not applicable; the data are included within this article.

Acknowledgments: We thank De In Kang and Korean Pharmacopuncture Institute for previous financial support, and Dong-Ho Cho, Sungcheol Hong, and Ho-Jong Chang for their research support in KAIST. In addition, we thank Eun-Sook Cho, Seung Hee Jeong from Seoul National University and Hyang Ran Yoon from Korea Research Institute of Bioscience and Biotechnology for their technical support and Hee Won Seo from KAIST for TOF-SIMS and Edward Button, Won-Hee Park for editing the manuscript and Ki-Young Lee for sample management.

Conflicts of Interest: The authors declare no conflict of interest.

References

1. Melino, G. The Sirens' song. *Nature* **2001**, *412*, 23. <https://doi.org/10.1038/35083653>.
2. Hotchkiss, R.S.; Strasser, A.; McDunn, J.E.; Swanson, P.E. Cell death. *N. Engl. J. Med.* **2009**, *361*, 1570-1583. <https://doi.org/10.1056/NEJMra0901217>.
3. Poon, I.K.; Lucas, C.D.; Rossi, A.G.; Ravichandran, K.S. Apoptotic cell clearance: basic biology and therapeutic potential. *Nat. Rev. Immunol.* **2014**, *14*, 166-180. <https://doi.org/10.1038/nri3607>.
4. Pittoni, V.; Valesini, G. The clearance of apoptotic cells: implications for autoimmunity. *Autoimmun Rev* **2002**, *1*, 154-161. [https://doi.org/10.1016/s1568-9972\(02\)00032-0](https://doi.org/10.1016/s1568-9972(02)00032-0).
5. Fond, A.M.; Ravichandran, K.S. Clearance of Dying Cells by Phagocytes: Mechanisms and Implications for Disease Pathogenesis. *Adv. Exp. Med. Biol.* **2016**, *930*, 25-49. https://doi.org/10.1007/978-3-319-39406-0_2.
6. Arandjelovic, S.; Ravichandran, K.S. Phagocytosis of apoptotic cells in homeostasis. *Nat. Immunol.* **2015**, *16*, 907-917. <https://doi.org/10.1038/ni.3253>.
7. Naora, H.; Montell, D.J. Ovarian cancer metastasis: integrating insights from disparate model organisms. *Nat. Rev. Cancer* **2005**, *5*, 355-366. <https://doi.org/10.1038/nrc1611>.
8. Langevin, H.M.; Yandow, J.A. Relationship of acupuncture points and meridians to connective tissue planes. *Anat. Rec.* **2002**, *269*, 257-265. <https://doi.org/10.1002/ar.10185>.
9. Langevin, H.M.; Churchill, D.L.; Wu, J.; Badger, G.J.; Yandow, J.A.; Fox, J.R.; Krag, M.H. Evidence of connective tissue involvement in acupuncture. *FASEB J.* **2002**, *16*, 872-874. <https://doi.org/10.1096/fj.01-0925fje>.
10. Stecco, C.; Sfriso, M.M.; Porzionato, A.; Rambaldo, A.; Albertin, G.; Macchi, V.; De Caro, R. Microscopic anatomy of the visceral fasciae. *J. Anat.* **2017**, *231*, 121-128. <https://doi.org/10.1111/joa.12617>.
11. Findley, T.W.; Shalwala, M. Fascia Research Congress evidence from the 100 year perspective of Andrew Taylor Still. *J Bodyw Mov Ther* **2013**, *17*, 356-364. <https://doi.org/10.1016/j.jbmt.2013.05.015>.
12. Joint Conference on Fascia, Acupuncture and Oncology, Joseph B. Martin Conference Center, Boston, Ma, USA, November, 2015.
13. Fede, C.; Fan, C.; Pirri, C.; Petrelli, L.; Biz, C.; Porzionato, A.; Macchi, V.; De Caro, R.; Stecco, C. The Effects of Aging on the Intramuscular Connective Tissue. *Int. J. Mol. Sci.* **2022**, *23*. <https://doi.org/10.3390/ijms231911061>.
14. Kim, B.H. Study on the reality of acupuncture meridians. *J. Jo Sun Med.* **1962**, *9*, 5-13.
15. Kim, B.H. On the Kyungrak system. *J. Acad. Med. Sci.* **1963**, *90*, 1-41.
16. Kim, B.H. The Kyungrak system. *J. Jo Sun Med.* **1965**, *108*, 1-38.

17. Lee, B.C.; Soh, K.S. A Novel Model for Meridian: Bonghan Systems Combined with Fascia (Bonghan-Fascia Model). In Proceedings of the Fascia Research II, Vrije Universiteit, Amsterdam, Netherlands, October 2009.
18. Shin, H.S.; Johng, H.M.; Lee, B.C.; Cho, S.I.; Soh, K.S.; Baik, K.Y.; Yoo, J.S.; Soh, K.S. Feulgen reaction study of novel threadlike structures (Bonghan ducts) on the surfaces of mammalian organs. *Anat. Rec. B. New Anat.* **2005**, *284*, 35-40. <https://doi.org/10.1002/ar.b.20061>.
19. Lee, B.C.; Yoo, J.S.; Ogay, V.; Kim, K.W.; Dobberstein, H.; Soh, K.S.; Chang, B.S. Electron microscopic study of novel threadlike structures on the surfaces of mammalian organs. *Microsc. Res. Tech.* **2007**, *70*, 34-43. <https://doi.org/10.1002/jemt.20383>.
20. Sung, B.; Kim, M.S.; Lee, B.C.; Yoo, J.S.; Lee, S.H.; Kim, Y.J.; Kim, K.W.; Soh, K.S. Measurement of flow speed in the channels of novel threadlike structures on the surfaces of mammalian organs. *Sci. Nat.* **2008**, *95*, 117-124. <https://doi.org/10.1007/s00114-007-0300-9>.
21. Yoo, J.S.; Ayati, M.H.; Kim, H.B.; Zhang, W.B.; Soh, K.S. Characterization of the primo-vascular system in the abdominal cavity of lung cancer mouse model and its differences from the lymphatic system. *PLoS One* **2010**, *5*, e9940. <https://doi.org/10.1371/journal.pone.0009940>.
22. Fujiwara, S.; Yu, S.B. 'Bonghan theory' morphological studies. *Igaku no Ayumi* **1967**, *60*, 567-577.
23. Lee, B.C.; Kim, K.W.; Soh, K.S. Visualizing the network of Bonghan ducts in the omentum and peritoneum by using Trypan blue. *J Acupunct Meridian Stud* **2009**, *2*, 66-70. [https://doi.org/10.1016/S2005-2901\(09\)60017-0](https://doi.org/10.1016/S2005-2901(09)60017-0).
24. Islam, M.A.; Thomas, S.D.; Sedoris, K.J.; Slone, S.P.; Alatassi, H.; Miller, D.M. Tumor-associated primo vascular system is derived from xenograft, not host. *Exp. Mol. Pathol.* **2013**, *94*, 84-90. <https://doi.org/10.1016/j.yexmp.2012.09.004>.
25. Bastos, A.L.; Marques, D.; Affra, M.A. Dye-induced fluorescence of tumour cells: photochemical action spectra. *Histochem. J.* **1974**, *6*, 237-243. <https://doi.org/10.1007/BF01312243>.
26. Michaelis, L. Die vitale Färbung, eine Darstellungsmethode der Zellgranula. *Arch. f. mikrosk. Anat.* **1899**, *55*, 558-575. <https://doi.org/10.1007/BF02977747>.
27. Yack, J.E. Janus Green B as a rapid, vital stain for peripheral nerves and chordotonal organs in insects. *J. Neurosci. Methods* **1993**, *49*, 17-22. [https://doi.org/10.1016/0165-0270\(93\)90105-z](https://doi.org/10.1016/0165-0270(93)90105-z).
28. Lee, B.C.; Yoo, J.S.; Baik, K.Y.; Kim, K.W.; Soh, K.S. Novel threadlike structures (Bonghan ducts) inside lymphatic vessels of rabbits visualized with a Janus Green B staining method. *Anat. Rec. B. New Anat.* **2005**, *286*, 1-7. <https://doi.org/10.1002/ar.b.20076>.
29. Lazarow, A.; Cooperstein, S.J. Studies on the mechanism of Janus green B staining of mitochondria. I. Review of the literature. *Exp. Cell Res.* **1953**, *5*, 56-69. [https://doi.org/10.1016/0014-4827\(53\)90094-9](https://doi.org/10.1016/0014-4827(53)90094-9).
30. Neradil, J.; Veselska, R.; Svoboda, A. The role of actin in the apoptotic cell death of P19 embryonal carcinoma cells. *Int. J. Oncol.* **2005**, *27*, 1013-1021. <https://doi.org/10.3892/ijo.27.4.1013>.
31. Choi, J.J.; Reich, C.F., 3rd; Pisetsky, D.S. The role of macrophages in the in vitro generation of extracellular DNA from apoptotic and necrotic cells. *Immunology* **2005**, *115*, 55-62. <https://doi.org/10.1111/j.1365-2567.2005.02130.x>.
32. Sonawane, S.; Khanolkar, V.; Namavari, A.; Chaudhary, S.; Gandhi, S.; Tibrewal, S.; Jassim, S.H.; Shaheen, B.; Hallak, J.; Horner, J.H.; et al. Ocular surface extracellular DNA and nuclease activity imbalance: a new paradigm for inflammation in dry eye disease. *Investig. Ophthalmol. Vis. Sci.* **2012**, *53*, 8253-8263. <https://doi.org/10.1167/iovs.12-10430>.
33. Gorczyca, W.; Bruno, S.; Darzynkiewicz, R.; Gong, J.; Darzynkiewicz, Z. DNA strand breaks occurring during apoptosis - their early insitu detection by the terminal deoxynucleotidyl transferase and nick translation assays and prevention by serine protease inhibitors. *Int. J. Oncol.* **1992**, *1*, 639-648. <https://doi.org/10.3892/ijo.1.6.639>.
34. Kim, J.H.; Kim, J.H.; Ahn, B.J.; Park, J.H.; Shon, H.K.; Yu, Y.S.; Moon, D.W.; Lee, T.G.; Kim, K.W. Label-free calcium imaging in ischemic retinal tissue by TOF-SIMS. *Biophys. J.* **2008**, *94*, 4095-4102. <https://doi.org/10.1529/biophysj.107.119800>.
35. Yip, W.L. Influence of oxygen on wound healing. *Int Wound J* **2015**, *12*, 620-624. <https://doi.org/10.1111/iwj.12324>.
36. Panchision, D.M. The role of oxygen in regulating neural stem cells in development and disease. *J. Cell. Physiol.* **2009**, *220*, 562-568. <https://doi.org/10.1002/jcp.21812>.

37. Kerr, J.F.; Wyllie, A.H.; Currie, A.R. Apoptosis: a basic biological phenomenon with wide-ranging implications in tissue kinetics. *Br. J. Cancer* **1972**, *26*, 239-257. <https://doi.org/10.1038/bjc.1972.33>.
38. Guicciardi, M.E.; Malhi, H.; Mott, J.L.; Gores, G.J. Apoptosis and necrosis in the liver. *Compr. Physiol.* **2013**, *3*, 977-1010. <https://doi.org/10.1002/cphy.c120020>.
39. Wen, S.; Ling, Y.; Yang, W.; Shen, J.; Li, C.; Deng, W.; Liu, W.; Liu, K. Necroptosis is a key mediator of enterocytes loss in intestinal ischaemia/reperfusion injury. *J. Cell. Mol. Med.* **2017**, *21*, 432-443. <https://doi.org/10.1111/jcmm.12987>.
40. Degterev, A.; Huang, Z.; Boyce, M.; Li, Y.; Jagtap, P.; Mizushima, N.; Cuny, G.D.; Mitchison, T.J.; Moskowitz, M.A.; Yuan, J. Chemical inhibitor of nonapoptotic cell death with therapeutic potential for ischemic brain injury. *Nat. Chem. Biol.* **2005**, *1*, 112-119. <https://doi.org/10.1038/nchembio711>.
41. Nikolettou, V.; Markaki, M.; Palikaras, K.; Tavernarakis, N. Crosstalk between apoptosis, necrosis and autophagy. *Biochim Biophys Acta Mol Cell Res* **2013**, *1833*, 3448-3459. <https://doi.org/10.1016/j.bbamcr.2013.06.001>.
42. Chan, F.K.; Luz, N.F.; Moriwaki, K. Programmed necrosis in the cross talk of cell death and inflammation. *Annu. Rev. Immunol.* **2015**, *33*, 79-106. <https://doi.org/10.1146/annurev-immunol-032414-112248>.
43. Segawa, K.; Nagata, S. An Apoptotic 'Eat Me' Signal: Phosphatidylserine Exposure. *Trends Cell Biol.* **2015**, *25*, 639-650. <https://doi.org/10.1016/j.tcb.2015.08.003>.
44. Tsujioka, T.; Yokoi, A.; Itano, Y.; Takahashi, K.; Ouchida, M.; Okamoto, S.; Kondo, T.; Suemori, S.; Tohyama, Y.; Tohyama, K. Five-aza-2'-deoxycytidine-induced hypomethylation of cholesterol 25-hydroxylase gene is responsible for cell death of myelodysplasia/leukemia cells. *Sci. Rep.* **2015**, *5*, 16709. <https://doi.org/10.1038/srep16709>.
45. Langevin, H.M.; Keely, P.; Mao, J.; Hodge, L.M.; Schleip, R.; Deng, G.; Hinz, B.; Swartz, M.A.; de Valois, B.A.; Zick, S.; et al. Connecting (T)issues: How Research in Fascia Biology Can Impact Integrative Oncology. *Cancer Res.* **2016**, *76*, 6159-6162. <https://doi.org/10.1158/0008-5472.CAN-16-0753>.
46. Olsen, G. Removal of Fascia--Cause of More Frequent Metastases of Malignant Melanomas of the Skin to Regional Lymph Nodes? *Cancer* **1964**, *17*, 1159-1164. [https://doi.org/10.1002/1097-0142\(196409\)17:9<1159::aid-cnrcr2820170910>3.0.co;2-8](https://doi.org/10.1002/1097-0142(196409)17:9<1159::aid-cnrcr2820170910>3.0.co;2-8).

Disclaimer/Publisher's Note: The statements, opinions and data contained in all publications are solely those of the individual author(s) and contributor(s) and not of MDPI and/or the editor(s). MDPI and/or the editor(s) disclaim responsibility for any injury to people or property resulting from any ideas, methods, instructions or products referred to in the content.